Unimolecular Reaction Rate Theory for Transition States of Any Looseness. 3. **Application to Methyl Radical Recombination**

David M. Wardlaw[†]

Department of Chemistry, Queen's University, Kingston, Ontario K7L 3N6, Canada

and R. A. Marcus*

Arthur Amos Noves Laboratory of Chemical Physics. California Institute of Technology, Pasadena, California 91125 (Received: March 25, 1986)

The theory for unimolecular reactions described in part 1 is applied to the recombination of methyl radicals in the high-pressure limit. The model potential energy surface and the methodology are briefly described. Results are presented for the recombination rate constant k_{∞} at T = 300, 500, 1000, and 2000 K. Canonical and Boltzmann-averaged microcanonical values of k_{∞} are compared, and the influence of a potential energy interpolation parameter and a separation-dependent symmetry correction on k_{∞} are examined. Earlier theoretical models and extensive experimental results are compared with the present results which are found to have a negative temperature dependence. The present results agree well with some of the available but presently incomplete experimental determinations of the high-pressure recombination rate constant for this reaction over the 300-2000 K temperature range. There is also agreement with a decomposition rate constant for a vibrationally excited ethane molecule produced by chemical activation.

I. Introduction

Bimolecular association reactions that have no energy barrier along the reaction coordinate have posed an interesting challenge in the theory of unimolecular reactions. These and related reactions were considered in parts 1^{1a} and 2^{1b} of this series. In the present paper these considerations are applied to the recombination of methyl radicals

$$2CH_3 \xrightarrow{k} C_2H_6 \tag{I.1}$$

where the recombination rate constant k is defined by

$$-\frac{d[CH_3]}{dt} = 2k[CH_3]^2$$
 (I.2)

For this reaction there is no barrier to the association along the reaction coordinate and a transition state is therefore not readily identifiable on that particular basis. There is, however, a "bottleneck" for such reactions in terms of the number of states as a function of the reaction coordinate,² and this bottleneck identifies the transition state. A method presented in part 1 and described in detail in part 2 has been given for implementing RRKM theory for such reactions.

In the present paper attention is focused on the methyl recombination reaction, in part because it has been extensively studied experimentally and its high-pressure value of k has been reported, according to the results of a number of authors, to display a negative temperature dependence. The latter is not predicted by some of the earlier theoretical models, described later. (The Gorin model, for example, predicts a k proportional to $T^{1/6}$.) This paradox posed by the earlier calculations stimulated our own interest in the problem. The reaction also serves to demonstrate the utility of the present method for treating systems involving the recombination of, or dissociation into, polyatomic fragments.

The high-pressure recombination rate constant k_{∞} is given as a function of the temperature T by³

$$k_{\infty}(T) = \frac{g_{\rm c}}{hQ_{\rm r}(T)} \int_0^{\infty} dE \sum_{J=0}^{\infty} (2J+1) N_{EJ}(R^{\dagger}) e^{-E/kT}$$
 (I.3)

where J is the total angular momentum quantum number, E is the total energy (in the center-of-mass frame), $N_{EJ}(R)$ is the sum of quantum states in all degrees of freedom except the reaction coordinate R for the given J and having energy less than or equal to E, R^{\dagger} is that value of R which minimizes N_{EJ} for a given (E, J) pair; Q_r is the partition function (in the center-of-mass frame) for the reactant fragments at infinite separation; and ge is the ratio g^{\dagger}/g_1g_2 of electronic partition functions for the transition state and separated radicals and is taken to be 1/4, corresponding to the usual approximation that only systems initially on the singlet potential energy surface can lead to recombination products.

The principal idea in the calculation of N_{EJ} , described in part 1, is that the degrees of freedom are subdivided into "transitional" ones and the remaining coordinates. The transitional degrees of freedom involve (a) the free rotations of the reactants which become bending and torsional motions of the product, (b) the relative orbital motion of the approaching fragments, and (c) the other coordinates, if any, which change considerably their form of motion during the approach along the reaction coordinate. The motions (a) to (c) are typically strongly coupled to each other and are constrained by energy and total angular momentum conservation, rendering formidable a purely quantum-mechanical calculation of the energy levels at each value of the reaction coordinate (so as to calculate $N_{EJ}(R)$). The density of states for such coordinates as a function of their energy ϵ , $\Omega_I(\epsilon)$, can sometimes be approximated, as we shall do here, by the corresponding classical phase-space integral.

With this subdivision of the coordinates N_{EJ} can be written as the convolution1

$$N_{EJ} = \int_0^E N_{\nu}(E - \epsilon) \ \Omega_J(\epsilon) \ d\epsilon \tag{I.4}$$

where $\Omega_J(\epsilon)$ de is the number of states of the transitional modes for the given J when their total energy lies in the interval (ϵ, ϵ) + de) and $N_{\nu}(E-\epsilon)$ is the number of quantum states in the remaining coordinates when their energy is less than or equal to $E - \epsilon$. The two types of coordinates are taken to be uncoupled

[†] NSERC of Canada University Research Fellow.

[‡]Contribution no. 7395.

^{(1) (}a) Wardlaw, D. M.; Marcus, R. A. Chem. Phys. Lett. 1984, 110, 230. (b) Wardlaw, D. M.; Marcus, R. A. J. Chem. Phys. 1985, 83, 3462. (2) Marcus, R. A. J. Chem. Phys. 1966, 45, 2630. Cf. comment on this paper in the introduction to ref 1a. Some later references to this criterion, namely to the work of M. Quack and J. Troe, W. L. Hase, B. C. Garrett and D. G. Truhlar are cited in ref 1a. D. G. Truhlar, are cited in ref 1a.

⁽³⁾ Marcus, R. A. J. Chem. Phys. 1965, 43, 2658. Equation I.3 is a straightforward adaptation of the unimolecular case treated in this reference.

from each other in eq I.4, apart from an indirect coupling via the dependence of the molecular structure and potential parameters on the reaction coordinate. The value of N_V in eq I.4 is obtained by the usual quantum count, 46 while $\Omega_f(\epsilon)$ and N_{EJ} are evaluated in the by Monte Carlo methods. The quantity $\Omega_J(\epsilon)$ is evaluated in the present paper by using action-angle variables, as in parts 1 and

Before presenting the calculations in some detail, it is useful to indicate qualitatively how the theory can lead to a negative temperature dependence of k_{∞} . In the case of a loose transition state (or, as it is sometimes known, the Gorin model) the transition-state location is determined by a balance of centrifugal and long-range van der Waals dispersion forces, free internal rotations are assumed, and the predicted k_{∞} is found to increase with T, varying as $T^{1/6}$. When, as in the present model, a more accurate treatment of the internal degrees of freedom is employed, the close spacing of their energy levels at large R (free rotations, for example) in contrast with the wider spacing at smaller R (restricted rotations now) causes $N_{EJ}(R)$ to be larger at large R than at somewhat smaller R's and thereby shifts the minimum of the $N_{EJ}(R)$ vs. R curve to an R^{\dagger} less than its value for the loose transition state. For the present model of $N_{EJ}(R)$ this shift increases as the energy is increased and, hence, as the temperature is increased. (The effect is enhanced with increasing energy, since at each R the number of states grows rapidly with the energy.) As R^{\dagger} decreases so does $N_{EJ}(R^{\dagger})$ relative to its loose value and so, thereby, does the rate constant. Accordingly, the deviations of the rate constant from the $T^{1/6}$ dependence should increase with T and, in this case, to such an extent that k_{∞} now decreases with

Other discussions of the decrease in R[†] with increasing temperature or increasing energy, based on the hindered rotor nature of some internal degrees of freedom, have been given by a number of authors.5 Several of these authors have also discussed the temperature dependence of the rate constant.5

The present article is divided as follows: In section II actionangle coordinates are given for the transitional modes; the transformation to the internal or relative coordinates is described in Appendix A. The potential energy function is presented and briefly discussed in section III and in Appendix B. The explicit evaluation of eq I.3 for the rate constant k_{∞} is described in section IV, and results are given in section V. A comparison of the recombination results with extensive experimental data and with earlier theoretical models is given in section VI; also included is a comparison with an experimental decomposition rate constant for vibrationally excited ethane produced by chemical activation. A summary and discussion follow in section VII.

II. Action-Angle Variables and Expression for N_{EJ}

In the description of these quantities we extract from part 22 only the material needed for a brief presentation of the method as it applies to methyl radical recombination. More detail and generality are given in part 2. Except where noted, both here and in Appendix A, the coordinate systems and transformations used are the same as those described earlier (Appendix E of part 2).

We label the two methyl radicals X_1 and X_2 and let (x, y, z)denote a set of Cartesian coordinate axes fixed in the combined X₁...X₂ system, the z axis being chosen to lie along the relative

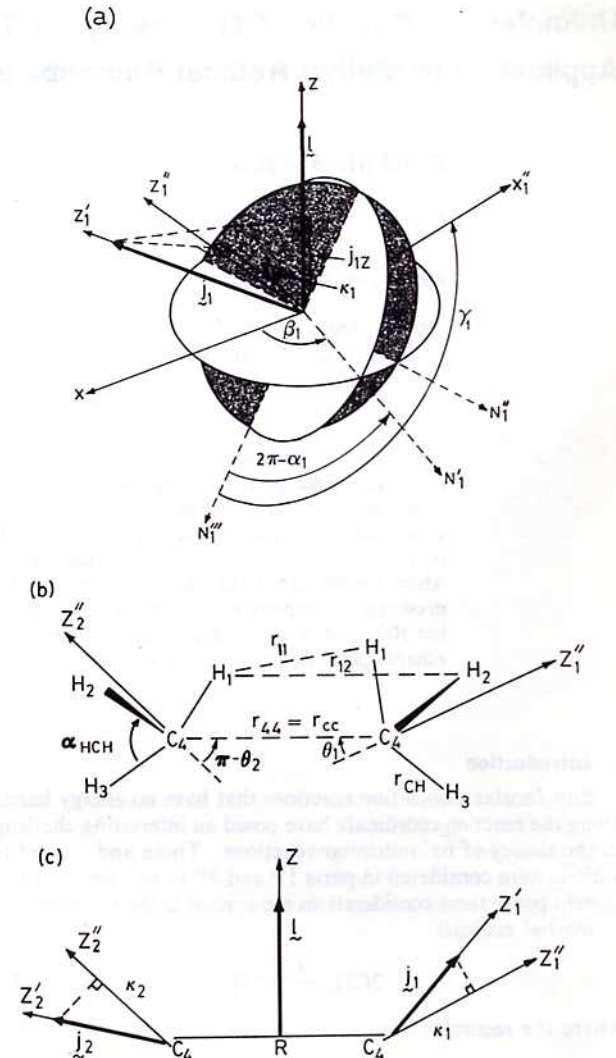


Figure 1. (a) Euler diagram depicting the relationship between the (x, y, z), (x_1', y_1', z_1') and (x_1'', y_1'', z_1'') Cartesian coordinate systems for the nonlinear polyatomic fragment 1. The doubly primed system is chosen so that the inertial tensor is diagonal in it; the zi" axis is the symmetry axis of the symmetric top methyl radical. I lies along the z axis, \mathbf{j}_1 lies along the z_1' axis, and κ_1 is the projection of \mathbf{j}_1 on the z_1'' axis. Pairs of the three planes intersect along the lines of nodes N_1' , N_1'' , and N_1 ", whose orientations are determined by the vectors $1 \times j_1$, $1 \times \kappa_1$, and $\kappa_1 \times \mathbf{j}_1$, respectively; N_1''' also serves as the x_1' axis. The angles (α_1, θ_n) β_1) are the Euler angles specifying the orientation of the primed system relative to the unprimed system, and the angles $(\gamma_1, \theta_{\kappa 1}, 0)$ are those specifying the orientation of the primed system relative to the doubly primed system. For pictorial clarity the angle θ_{II} between the z axis and the z_1' axis and the angle θ_{x1} between the z_1' axis and the z_1'' axis are not shown. (b) The CH bond length r_{CH} , the angle between adjacent CH bonds α_{HCH} , the bond dissociation/association coordinate $r_{CC} = r_{44}$, several interfragment atomic separation coordinates r_{ij} , and the angles θ_i between r_{CC} and the symmetry axis z_i'' of fragment i (i = 1, 2) for the CH3...CH3 system. The carbon atom of fragment 2 is taken as the origin of rcc. (c) Angular momenta for fragment rotations and for the orbital motion of CH3...CH3, the distance R between the centers of mass, and the projection κ_i of j_i on the $z_i^{\prime\prime}$ axis.

orbital angular momentum vector I of the two fragments as in Figure 1a. (Throughout angular momentum actions are written in units of h = 1.) In the present paper the x axis is chosen to lie along the vector $\mathbf{l} \times \mathbf{j}_i$, where \mathbf{j}_i is the rotational angular momentum vector of X_i (i = 1, 2). In part 2 it lies instead along the vector $\mathbf{l} \times \mathbf{k}$, where \mathbf{k} is an intermediate angular momentum vector defined to be $j_1 + j_2$. (This new x axis reduces somewhat the computational effort involved in the transformation from action angle to internal coordinates. The new details are given in Appendix A.) The relative separation vector R along the line joining the centers of mass of the two fragments lies in the body-fixed

^{(4) (}a) This $N_V(E-\epsilon)$ is equivalent to the $N_V(E'-\epsilon)$ in ref 1: The present $N_V(E-\epsilon)$ is zero until $E-\epsilon$ exceeds $V_{\min}(R)+E_{zp}(R)$, where $V_{\min}(R)$ is the potential energy minimum at that R and $E_{zp}(R)$ is the zero-point energy of the "conserved degrees of freedom" at that R. The previous $N_V(E'-\epsilon)$ was zero until $E'-\epsilon$ exceeded zero. The E' in ref 1 equals $E-V_{\min}(R)-E_{zp}(R)$. (b) A grid size of 2 cm-1 was used to obtain an approximate direct count via the approach described in part 2 where a grid size of 1 cm-1 was employed. R_{EJ} results for these two grid sizes at various R values for a high energy $(E - E_{Tp} = 63.52 \text{ keal mol}^{-1})$ were found to agree within the statistical uncertainty (represented by σ^{MC}) imposed by the Monte Carlo calculation. The larger grid size of 2 cm⁻¹ reduces both the computer memory requirement and the execution time of an N_{EJ} calculation.
(5) E.g.: Hase, W. L. J. Chem. Phys. 1976, 64, 2442. Quack, M.; Troe,

J. Ber. Bunsenges. Phys. Chem. 1977, 81, 329. Smith, G. P.; Golden, D. M. Int. J. Chem. Kinet. 1978, 19, 489. Benson, S. W. Can. J. Chem. 1983, 64,

Methyl Radical Recombination

in Figure 1a.

xy plane and is oriented at an angle α_l with respect to the x axis (α_l is conjugate to l). The vector **R** and the angle α_l are not shown

Two coordinate frames (x_i', y_i', z_i') and (x_i'', y_i'', z_i'') are fixed in fragment X_i and are defined as in Figure 1a and in the caption to that figure. The projections of j_i on the z_i and z_i'' axes are

denoted by j_{iz} and κ_i , respectively (Figure 1a). The angles conjugate to (j_i, j_{iz}, κ_i) are $(\alpha_i, \beta_i, \gamma_i)$, respectively (Figure 1a). The z projection of I, l_z , its conjugate angle β_l , and α_l specify the orientation of the body-fixed (x, y, z) system with

respect to a space-fixed system. These coordinates provide a set of variables $(l, \alpha_l, l_z, \beta_l, j_1, \alpha_1, j_{1z}, \beta_1, \kappa_1, \gamma_1, j_2, \alpha_2, j_{2z}, \beta_2, \kappa_2, \gamma_2)$ which specify, among other things, the orientation in space of each β_2) the variables $(J, J_z, k, \alpha, \beta, \alpha_k)$ will be used, where J_z is the

z projection of **J** and the angles α , β , α_k are conjugate to J, J_z , k, respectively. The resulting action variables are J, J_z , j_1 , j_2 , k, l, κ_1, κ_2 and their respective conjugate angles are $\alpha, \beta, \alpha_1, \alpha_2, \alpha_k$ α_l , γ_1 , γ_2 . The reaction coordinate R, the angular momenta j_1 , j_2 , l, and the projections κ_1 , κ_2 are depicted in Figure 1c. The expression for $\Omega_f(\epsilon)$ in terms of these action-angle variables

 $\Omega_{J}(\epsilon) = (2\pi)^{-8} \sigma^{-1} \int \dots \int \mathrm{d}J_{z} \, \mathrm{d}j_{1} \, \mathrm{d}j_{2} \, \mathrm{d}k \, \mathrm{d}l \, \mathrm{d}\kappa_{1} \, \mathrm{d}\kappa_{2} \, \mathrm{d}\alpha \, \mathrm{d}\beta$ $\mathrm{d}\alpha_{1} \, \mathrm{d}\alpha_{2} \, \mathrm{d}\alpha_{k} \, \mathrm{d}\alpha_{l} \, \mathrm{d}\gamma_{1} \, \mathrm{d}\gamma_{2} \, \Delta(J,k,l) \, \Delta(k,j_{1},j_{2}) \, \delta(\epsilon-H_{\mathrm{cl}}) \, (\mathrm{II}.1)$ The limits on the angle variables are 0 to 2π , the J_z integral is over the interval (-J, J), the κ_i integrals are restricted by $|\kappa_i| \le$

 j_i , the angular momentum actions j_1 , j_2 , k, and l are restricted by the indicated triangle inequalities Δ and by energy conservation (Δ equals unity when the triangle inequalities are fulfilled and is zero otherwise), and σ is a symmetry number to be discussed in section IV. For $X_1 - X_2$ the Hamiltonian H_{cl} is written as

$$H_{\rm cl} = E_{\rm rl} + E_{\rm r2} + \frac{l^2}{2\mu R^2} + V_{\rm t}(r_{mn}, \theta_1, \theta_2) \qquad (II.2)$$
 where μ is the reduced mass for relative motion of the X_1 and X_2

fragments, V_t is the potential energy function for the transitional modes (i.e., for variation in the separation distance and in the orientation of the CH₃ groups), and r_{mn} (m, n = 1-4) denotes a 4×4 set of distances which, together with θ_1 and θ_2 , are described In the particular case of CH₃ fragments the principal moments

of inertia are related by $I_A = I_B < I_C$ and each CH₃ is an oblate symmetrical top with symmetry axis C and with I_r [= $I_AI_C/(I_A$

 $-I_{\rm C}$)] negative. We note that an additional restriction on $|\kappa_i|$ arises from the requirement that E_{ri} must be greater than or equal to

zero. The relation between the action-angle variables of eq II.1 and the internal coordinates r_{mn} , θ_1 , θ_2 for the case of CH₃···CH₃ is described in Appendix A. As seen in Appendix A, H_{cl} is independent of (J_z, α, β) and

 $\Omega_J(\epsilon) = (2J + 1)(2\pi)^{-6}\sigma^{-1}\int ... \int dj_1 dj_2 dk dl d\kappa_1 d\kappa_2 d\alpha_1$ $d\alpha_2 d\alpha_k d\alpha_l d\gamma_1 d\gamma_2 \Delta(J,k,l) \delta(k,j_1,j_2) \delta(\epsilon - H_{cl})$ (II.3)

and
$$N_{EJ} = (2J + 1)(2\pi)^{-6}\sigma^{-1}\int ... \int dj_1 dj_2 dl dk d\kappa_1 d\kappa_2 d\alpha_1 d\alpha_2 d\alpha_k d\alpha_l d\gamma_1 d\gamma_2 N_{\nu}(E - H_{cl}) \Delta(J,k,l) \Delta(k,j_1,j_2)$$
(II.4)

The evaluation of eq II.4 is described briefly in section IV. We shall use p (products) and r (reactants) subscripts to denote

properties of the molecule and of the fragments, respectively. In

particular E_{zp} will denote the total zero-point energy of the two

methyl radicals at $R = \infty$. III. Potential Energy Function

For the $2CH_3 \rightarrow C_2H_6$ reaction a model potential $V = V_c +$ V_t is used. This potential is intended to be physically reasonable but not quantitatively accurate since it is not constructed from ab initio points but, rather, is based on several different types of approximation, as described below. However, it is to be emTABLE I: Correlation of Conserved Vibrations^a C_2H_4

The Journal of Physical Chemistry, Vol. 90, No. 21, 1986

			C ₂ H ₆			C	H ₃
label		sym				sym	
i	mode	type	ν	ν_i^{p}	mode	type	$\nu_i^{\ r}$
1	ν_1	Alg	2954	2925.0	ν_1	A_1'	304
	ν_5	A _{2u}	2896				
2	ν_2	A_{1g}	1388	1383.5	ν_2	$A_2^{\prime\prime}$	58
	ν_6	A_{2u}	1379				
3	ν_7	$\mathbf{E}_{\mathbf{u}}$	2985	2977.0	ν_3	$\mathbf{E'}$	316
	ν_{10}	$\mathbf{E}_{\mathbf{g}}$	2969				
4	ν_8	$\mathbf{E}_{\mathbf{u}}^{T}$	1472	1470.5	ν_4	E'	139
	ν_{11}	$\mathbf{E}_{\mathbf{g}}$	1469				
^a All fr	equencies	are in	units of	cm ⁻¹ and	are take	n from	ref 8.
TABLE I	I: Disap	pearing	Vibratio	nal Mode	s of C ₂ H	6 ^a	
		syn	n				
n	node	typ	e	ν	de	scription	1

 ν_4

289 821

C-C stretch torsion CH₃ rock CH₃ rock

580

3162

1396

1206 ^a All frequencies are in cm⁻¹ and are taken from ref 8.

phasized that the utility of the present method is independent of the accuracy or explicit form of the potential energy surface.

modes in methyl fragments 1 and 2, in units of $\hbar = 1$:

The potential V_c is for the "conserved" vibrational degrees of freedom (listed in Table I) and is assumed for simplicity to be separable and quadratic. (Inclusion of approximate anharmonicity

corrections in the potential V_c would not lead to difficulties in obtaining the sum of states N_{ν} .^{6,7}) The vibrational energy in excess of the (R-dependent) zero-point energy is then expressed in terms of principal quantum numbers n_{i1} and n_{i2} of the normal

 $E_V = \sum_{i=1}^4 2\pi \nu_i(R) [n_{i1} + n_{i2}]$

The sum is over the (identical) vibrations of each methyl group,

two of which are doubly degenerate. For simplicity the frequencies

 $\nu_i(R)$ were obtained by interpolation

with

in Table II.

and is described in Appendix B.

interpolation parameter. It is not clear that the interpolation in

 $g(R) = \exp[-\alpha(R - R_e)]$

eq III.3 is physically correct; when an improved potential energy

surface becomes available, this approximation can be avoided. The

two particular values of α used in this work are discussed in section IV. The reactant frequencies v_i^r are the normal-mode frequencies of an isolated methyl radical and are listed with their symmetry

type in Table I. The product frequencies ν_i^p , which correlate to

the $v_i^{\rm r}$ via eq III.2, were determined as follows: For a given symmetry type (either A or E) and for each type of vibration (either CH₃ stretching or CH₃ deformation), two nearly degenerate

frequencies of C_2H_6 were averaged. The resultant ν_i^{p} 's were then correlated on a 1:1 basis with v_i^r 's according to symmetry type

and characteristic vibrational motion⁸ and are listed in Table I together with their symmetry type. The remaining normal modes

assumed to arise from nonbonded and bonded interactions

 $V_{\rm t} = V_{\rm NB} + V_{\rm B}$

 $v_i(R) = v_i^{\rm r} + (v_i^{\rm p} - v_i^{\rm r})g(R) \quad (i = 1, ..., 4)$

(III.2)

where R_e is the equilibrium value of R in C_2H_6 and α is an

(III.1)

of C₂H₆ arise from transitional modes as R decreases and are listed The potential V_t for the transitional degrees of freedom is

(III.4)

(6) Troe, J. J. Chem. Phys. 1983, 79, 6017.

(7) Bhuiyan, L. B.; Hase, W. L. J. Chem. Phys. 1983, 78, 5052.
(8) Quack, M.; Troe, J. Ber. Bunsenges. Phys. Chem. 1974, 78, 240.

The Journal of Physical Chemistry, Vol. 90, No. 21, 1986

TABLE III: Features of the Transitional Mode Potential V_t^a for $\alpha =$

1.0 Å ⁻¹				
R, Å	$V_{\min}(R)$	$V_{\text{tor}}(R)$	$V_{\rm barr}(R)$	$E_{\min}(R)$
2.2	-59.6	0.107	319.8	58.8
2.3	-51.0	0.069	190.6	50.3
2.4	-43.3	0.045	119.1	42.6
2.5	-36.4	0.029	77.8	35.8
2.6	-30.5	0.019	53.9	30.0
2.7	-25.5	0.011	38.9	25.0
2.8	-21.2	0.007	28.9	20.8
2.9	-17.6	0.005	21.9	17.3
3.0	-14.6	0.002	17.0	14.3
3.1	-12.1	0.001	13.5	11.8
3.2	-10.1	0.000	10.8	9.8

In order to assess certain features of the transitional mode

potential V_t , the latter was evaluated on a five-dimensional grid

or "back to face".

commented on in footnote 10.

1979, 52, 3242

of the angles $(\delta_1, \delta_2, \gamma_1, \gamma_2, \chi_2)$ for a set of R values ranging from 2.2 to 7.0 Å in 0.1-Å increments. The angles γ_1, γ_2 are conjugate to κ_1 , κ_2 and appear in eq II.1, II.3, and II.4, but the angles δ_1 , δ_2 , χ_2 are not conjugate to any angular momentum action variable appearing in section II. These five angles constitute the minimum number needed to specify the relative orientation of the two radicals and are described in Appendix C. They, together with the separation distance R, completely determine the arguments $(r_{mn}, \theta_1, \theta_2)$ of V_t . Also defined in Appendix C are three types of relative orientational configurations of the two methyl radicals, when each radical is in an umbrella-like configuration. Configuration A ("back to back") where the umbrellas are, as in ethane, facing away from each other is the most favorable one for reaction. In configuration C they are "face to face" and in B "face to back"

For each value of R in the interval 2.2–7.0 Å in increments of 0.1 Å and for both values of the interpolation parameter α , the absolute potential minimum $V_{\min}(R)$ occurred for the staggered "equilibrium" arrangement of configuration A, i.e., at $\delta_1 = 0$ and $\delta_2 = \pi$, $\chi_2 = \gamma_2 = 0$, and $\gamma_1 = \pi/3$. For $\alpha = 1.0 \text{ Å}^{-1}$ the quantity V_{\min} is given in Table III for values of R ranging from 2.2 to 3.2 Å. Local minima occur for configuration B with $\delta_1 = \delta_2 = 0$ or

 $\delta_1 = \delta_2 = \pi$ and configuration C with $\delta_1 = \pi$ or $\delta_2 = 0$. Also listed in Table III is a torsional barrier, $V_{tor}(R)$, defined as the difference in V_1 between the eclipsed arrangement ($\delta_1 = 0$, $\delta_2 = \pi$, $\gamma_1 = \gamma_2$ = χ_2 = 0) and the staggered arrangement (defined above) of configuration A. As expected, V_{tor} is a decreasing function of R. Semiempirical molecular orbital calculations for the potential energy between recombining methyl radicals by Yamabe, Minato, Fujimoto, and Fukui⁹ predict a small value of V_{tor} at $r_{\text{CC}} = 2.85$ Å, namely $V_{\text{tor}} = 0.37 \text{ kcal mol}^{-1}$. The present model for V_{t} yields an even smaller value, $V_{\text{tor}} = 0.047 \text{ kcal mol}^{-1}$, a discrepancy

(9) Yamabe, S.; Minato, T.; Fujimoto, H.; Fukui, K. Bull. Chem. Soc. Jpn.

tions A and B and lies near the boundary ($\delta_2 \sim \pi/2$) separating these two cases. V_{barr} is seen to decrease rapidly with increasing R for the smaller Rvalues and then to decrease more slowly as R further increases. For comparison with $V_{\rm barr}$ we list in column 5 the minimum available energy $E_{\rm min}(R)$,

i.e., the energy available at a given R value if $E - E_{zp} = 0$.

IV. Calculation of $k_{\infty}(T)$

In this section three related approaches to the calculation of the recombination rate constant are described, the second two being approximations to the first. In each case the reactant partition function $Q_r(T)$ appearing in the denominator of eq I.3 is the same and is obtained by modeling each methyl radical as a collection of separable harmonic oscillators and a rigid rotor. The general form of Q_r and pertinent details are found in ref 13; the CH3 vibrational frequencies are listed in Tables I and II, and the CH₃ moments of inertia are determined from data in Table III. The sum over J in the numerator of eq I.3 is replaced, in each case, by an integral whose lower limit is zero and whose upper limit is taken to be $J_{\text{max}}(E_0)$. Here J_{max} is the maximum value of J for a rigid symmetric top model of equilibrium C_2H_6 when all of the available product energy, $E - E_{zp} + D_0(C-C)$, is in the overall rotation of the C_2H_6 product (D_0 is listed in Table III). In the first approach, with a rate constant denoted by k_{∞}^{I} , a

transition state is determined at each E, and in the third approach (k_{m}^{III}) it is determined at each T, as described below. (i) k_{∞}^{I} . The integrals over E and J in eq I.3 are approximated by N-point Laguerre and 2M-point extended Simpson's rule quadratures, ¹⁴ respectively, yielding

transition state is determined for each E and J and the results

are then averaged over E and J by using the Boltzmann weighting

factor. This approach is the correct one for the present model as one sees from eq I.3. In the second approach (k_{∞}^{II}) the

$$k_{\infty}^{\text{I}}(T) = \frac{1}{g_{\text{e}}hQ_{\text{r}}(T)}kT\frac{\Delta J}{3}\sum_{i=1}^{N}\sum_{k=0}^{2M}w_{i}w_{k}N_{E,J_{k}}(R_{\text{l}}^{\dagger})$$
 (IV.1)

 ΔJ is the constant step size for the J quadature, $J_k = k\Delta J$, and $w_k = 1$ for k = 0 or 2M, $w_k = 2$ for k even, and $w_k = 4$ for k odd. The transition-state location R_1^{\dagger} is determined independently for each (E_i, J_k) pair in eq IV.1 by minimizing $N_{E_iJ_k}$ with respect to R on a 0.1- \mathring{A} grid over an appropriate range of R values. The integral appearing in the expression for N_{EJ} in eq II.4 is evaluated by the Monte Carlo method described in part 2 and will not be

where $E_i = kTx_i$, w_i and x_i are Laguerre weights and points, ¹⁴

discussed here. The Monte Carlo approximation to N_{EJ} is denoted $N_{EJ} \pm \sigma^{\rm MC}$, where $\sigma^{\rm MC}$ is one standard deviation. Estimates of the upper and lower bounds on $k_{\omega}^{\rm I}(T)$ are obtained by using $(N_{EJk} + \sigma^{\rm MC})$ and $(N_{EJk} - \sigma^{\rm MC})$, respectively, in eq IV.1. Since the present model potential $V_{\rm t}$ for the transitional modes admits, for sufficiently small values of R and E, disjoint regions A, B, C (defined earlier) of energetically accessible classical phase space, we have introduced an ad hoc restriction in the Monte Carlo sampling procedure. 15 The value of the symmetry factor σ in eq II.4 deserves special

large values of R_i^{\dagger} and hence essentially planar methyl radicals. In this case each of the identical fragments has both a C_{2n} and a C_{3v} axis resulting in $\sigma_l = (3 \times 2)^2 \times 2 = 72$. The results given in section V, apart from those labeled $k_{\infty}^{I'}$ and $k_{\infty}^{II'}$, were obtained by using this value of σ . Those designated $k_{\infty}^{I'}$ and $k_{\infty}^{II'}$ were

consideration. A loose transition state will be characterized by

originating with reactants $(R = \infty)$ and passing through $\Gamma(R)$ does not dynamically evolve to configuration A (via an inversion). It cannot so evolve classically via a rotation. Thereby, it cannot evolve to bound C_2H_6 product without recrossing the fixed R hypersurface. Such recrossings, although dynamically possible, are thereby explicitly excluded in the usual application of transition-state theory considered here.

^a All energies are in kcal mol⁻¹.

⁽¹⁰⁾ The authors of ref 9 note that their numbers "should be regarded as qualitative." However, in the equilibrium configuration for ethane $(R = R_c)$

^{= 1.70} Å) the present value of $V_{\text{tor}} = 0.83$ kcal mol⁻¹ is also too small, compared to the accepted value¹⁰ of ~ 3 kcal mol⁻¹. The latter result is not

surprising since the Lennard-Jones parameters used were not designed for such short distances (11) Chao, J.; Wilhoit, R. C.; Zwolinski, B. J. J. Phys. Chem. Ref. Data 1973, 2, 427.

⁽¹²⁾ For each triplet of angles $(\delta_1, \delta_2, \chi_2)$ the minimum value of V_1 , denoted by $V_1^{\min}(\delta_1, \delta_2, \chi_2)$, is selected from the (γ_1, γ_2) grid. Next, for fixed δ_1 and χ_2 , the minimum-energy path for flipping radical 2 (i.e., δ_2 progressing from 0 to π) with respect to radical 1 is defined by the set $\{V_1^{\min}(\delta_1, \chi_2; 0 \le \delta_2 \le \pi)\}$. The largest value of $V_{\text{barr}}(\delta_1, \chi_2)$ for all δ_1 and χ_2 is taken as the $V_{\text{barr}}(\delta_1, \chi_2)$ and the smallest value of $V_{\text{barr}}(\delta_1, \chi_2)$ for all δ_1 and χ_2 is taken as the V_{barr} entry in Table III. For all R values it is found that the interval of configurations δ_1 = 0 to $\pi/18$, $\delta_2 = 7\pi/18$ to $8\pi/18$, and $\chi_2 = 0$ to $\pi/9$ give rise to V_{barr} . That is, the lowest barrier to flipping occurs for the transition between configura-

In Table III is also given V_{barr} as a function of R. This quantity is the approximate minimum barrier height, as measured from the R-dependent absolute potential minimum, for the flipping of X_2 , by changing δ_2 , for a given orientation of X_1 . The role of V_{barr} in evaluating N_{EJ} is described in section IV. It is obtained from the angle-space grid of V_t values for each R value.

⁽¹³⁾ Weston, R. E.; Schwarz, H. A. Chemical Kinetics; Prentice-Hall: Englewood Cliffs, NJ, 1972 (14) Abramowitz, M.; Stegun, I. Handbook of Mathematical Functions;

Dover: New York, 1965; p 890.

⁽¹⁵⁾ If the available energy $E - E_{zp} + E_{min}$ is less than V_{barr} (see Table IV) for a given R value, then phase-space points $\Gamma(R)$ corresponding to configurations B or C are rejected on the assumption that a classical trajectory

TABLE IV: Values of k_{∞}^{-1} (Minimization at Each E and J)^a

temp, K	N	$\Delta J,~\hbar$	2 <i>M</i>	$k_{\infty}^{I} \pm \delta$, $10^{13} \text{ cm}^{3} \text{ mol}^{-1} \text{ s}^{-1}$
		$\alpha = 1$.0 Å ⁻¹	-
300	6	25	6	4.33 ± 0.12
	10	25	6	4.26 ± 0.12
	6	12.5	10	4.15 ± 0.10
500	6	25	8	3.67 ± 0.08
1000	6	25	8	2.37 ± 0.06
2000	6	25	10	1.09 ± 0.04
		$\alpha = 0$	0.8 Å⁻¹	
300	6	25	6	3.84 ± 0.08
2000	6	25	10	0.96 ± 0.03

^aN and 2M denote the number of i points and k points in the sums of eq IV.1, respectively; ΔJ denotes the step size in the J_k quadrature in eq IV.1; $k_{\infty}^{-1} = \frac{1}{2}[(k_{\infty}^{-1})_{\max} + (k_{\infty}^{-1})_{\min}]$ and $\delta = \frac{1}{2}[(k_{\infty}^{-1})_{\max} - k_{\infty}^{-1})_{\min}]$, where $(k_{\infty}^{-1})_{\max}$ and $(k_{\infty}^{-1})_{\min}$ are estimated upper and lower bounds obtained by using $N_{E,J_k} + \sigma^{MC}$ and $N_{E,J_k} - \sigma^{MC}$, respectively, in

obtained by an approximate interpolation taking into account the umbrella shape of the methyl radicals at smaller R values. 16 (ii) k_{∞}^{II} . By defining

$$N_{\rm E}(R) = \int_0^{J_{\rm max}} \mathrm{d}J \ N_{EJ}(R) \tag{IV.2}$$

and approximating the integral over E by an N-point Laguerre quadrature, we obtain the following approximation to eq I.3.

$$k_{\infty}^{\text{II}}(T) = \frac{1}{g_{c}hQ_{r}(T)}kT\sum_{i=1}^{N}w_{i}N_{E_{i}}(R_{\text{II}}^{\dagger})$$
 (IV.3)

In contrast to (i) the transition state location R_{II}^{\dagger} is determined for each E_i in eq IV.3 by minimizing N_{E_i} with respect to R on a 0.1-Å grid. The integral for N_E in eq IV.2 is evaluated by modifying the Monte Carlo method described in part 2 to include the additional integration over J. $k_{\infty}^{II}(T)$ will exactly equal $k_{\infty}^{I}(T)$ only when R_1^{\dagger} is independent of J. As in (i), phase-space points corresponding to configurations B and C are excluded from $N_{\rm E}$ if $E < V_{\text{barr}}$ (see footnote 15, Table IV). Recombination rate constants k_{∞}^{II} , analogous to k_{∞}^{I} , are also considered in section V and are obtained by substituting N_{E_i} for N_{E_i} in the expressions in footnote 16, so yielding N_{E_i} .

(iii) k_{∞}^{III} . This canonical rate constant is taken to be

$$k_{\infty}^{\text{III}}(T) = \frac{1}{g_{\text{e}}hQ_{\text{r}}(T)}kT[\sum_{i=1}^{N}w_{i}N_{E_{i}}]_{R_{\text{III}}\dagger}$$
(IV.4)

where the transition-state location $R_{\rm III}^{\dagger}$ is determined by minimizing the sum $\sum_i w_i N_{E_i}$ with respect to R on a 0.2-Å grid; this value of R_{III}^{\dagger} is thereby independent of E_i . The evaluation of N_{E_i} in eq IV.4 is described in (ii). k_{∞}^{III} will equal k_{∞}^{I} exactly only if R_{I}^{\dagger} is independent of both E and J. k_{∞}^{III} has, in effect, also been used in earlier literature of reactions (maximization of free entropy of activation, sometimes known now as canonical variational transition-state theory).

V. Results for k_{∞} 's, R^{\dagger} 's, and Configurational Populations

Results are given for k_{∞}^{I} in Table IV for the four temperatures 300, 500, 1000, and 2000 K, which span the temperature range studied in the collective experimental work. The majority of results

$$N_{E,J_k}' = pN_{E,J_k} + (1-p)4N_{E,J_k}^{A}$$

where $N_{E_iJ_k}^{}$ includes only states corresponding to configuration A and both $N_{E_iJ_k}$ and $N_{E_iJ_k}^{}$ are obtained by using $\sigma=\sigma_i$ in eq II.4, with a weighting factor p given as follows. A weighting function p was chosen which becomes zero at $R=R_c$ and unity at $R=\infty$. In as much as $N_{E_iJ_k}^{} = N_{E_iJ_k}$ when $R=R_c$ and $N_{E_iJ_k}^{} = 1/4N_{E_iJ_k}$ when $R=\infty$, a suitable p is

$$p = \frac{4}{3}(N_{E,J_k} - N_{E,J_k}^{A}) / N_{E,J_k}$$

TABLE V: Dependence of R_1^{\dagger} , $N_{EJ}(R_1^{\dagger})$, and $N_{EJ}(R_1^{\dagger})/N_{EJ}(\infty)$ on E and J for $\alpha = 1.0 \text{ Å}^{-1}$

and J for α	= 1.0 A			
$E - E_{zp}$, kcal mol ⁻¹	J, ħ	$R_{ m I}^{\dagger,a}$ Å	$N_{EJ}(R_{ m I}^{\dagger})$	$N_{EJ}(R_{ m i}^{\dagger})/N_{EJ}(\infty)$
0.13	0	100.0	0.33×10^{2}	1.0
0.15	25	5.6-5.8	0.24×10^{1}	0.02
	50	2,0 2,0	b	
	100		b	
	150		b	
0.44	0	100.0	0.67×10^{3}	1.0
0.77	25	5.2-6.0	0.20×10^4	0.47
	50	3. 2 0.0	b	
	100		b	
	150		b	
1.18	0	6.6-7.0	0.78×10^4	0.99
1.10	25	5.6	0.62×10^{5}	0.76
	50	4.4	0.81×10^4	0.10
	100		b	
	150		b	
2.36	0	3.7-3.8	0.46×10^{5}	0.96
2.00	25	3.7-3.9	0.60×10^6	0.86
	50	3.9-4.1	0.20×10^6	0.29
	100	_	b	
	150		b	•
4.73	0	3.5-3.6	0.31×10^{6}	0.67
	25	3.5-3.7	0.59×10^{7}	0.68
	50	3.5-3.7	0.29×10^7	0.33
	100	3.7	0.50×10^{5}	0.01
	150		b	
9.53	0	3.3	0.42×10^7	0.46
	25	3.3-3.4	0.10×10^{9}	0.47
	50	3.3-3.4	0.63×10^{8}	0.29
	100	3.4	0.59×10^{7}	0.03
	150		b	
19.55	0	3.0-3.1	0.15×10^9	0.27
	25	3.0-3.2	0.48×10^{10}	0.30
	50	3.1-3.2	0.35×10^{10}	0.21
	100	3.1	0.65×10^{9}	0.04
	150	3.0-3.1	0.24×10^{8}	<0.01
39.10	0	2.8	0.14×10^{11}	0.15
	25	2.8	0.52×10^{12}	0.15
	50	2.8	0.48×10^{12}	0.13
	100	2.8	0.15×10^{12}	0.04
	150	2.7-2.8	0.16×10^{11}	<0.01
63.52	0	2.5	0.59×10^{12}	0.09
	25	2.6-2.7	0.29×10^{14}	0.09
	50	2.6	0.28×10^{14}	0.07
	100	2.5-2.6	0.10×10^{14}	0.03
	150	2.5-2.6	0.19×10^{13}	<0.01

^a A range of R_1^{\dagger} values indicates that the associated $N_{EJ}(R_1^{\dagger})$ values agree to within their Monte Carlo uncertainty. ${}^bN_{EJ}$ is zero over a range of R values and no $R_{\rm I}^{\dagger}$ value can be assigned; these J's do not

were obtained with a value^{8,17,18} of 1.0 Å⁻¹ for the parameter α appearing in eq III.3. A limited set of results with $\alpha = 0.8 \text{ Å}^{-1}$ is also included, close to the value of 0.82 Å⁻¹ determined by Hase¹⁹ by fitting a different variational transition-state model to experimental rate data. Table IV also contains some results with different numbers of quadrature points. The number 2M for the J integration was chosen such that the contribution of the term with k = 2M in eq IV.1 was essentially zero.

At all four temperatures and for all values of (E_i, J_k) in eq IV.1 a minimum in the N_{E,J_k} vs. R grid was readily identifiable for both values of α . As is noted in part 2, the relative error in $N_{E,J}$ increases as R decreases for a given number of Monte Carlo integration points. Since increasing the number of Monte Carlo points to maintain a constant σ^{MC}/N_{EJ} as R decreases requires excessive computer time, this was not done. Instead, a smaller increase in the number of points was adopted and a slow but steady increase in σ^{MC}/N_{EJ} with decreasing R was accepted with no adverse effects on the overall calculation.

⁽¹⁶⁾ For a tight transition state with smaller $R_{\rm I}^{\dagger}$ the methyl radicals are no longer planar but have an umbrella shape. Consequently, there is no C_{2v} axis and $\sigma_1 = 3^2 \times 2 = 18 = \sigma_1/4$. We therefore also consider recombination rates, denoted $k_{\infty}^{I'}$, estimated from an approximate interpolation

⁽¹⁷⁾ Troe, J. J. Phys. Chem. 1984, 88, 4375.

⁽¹⁸⁾ Cobos, C. J.; Troe, J. J. Chem. Phys. 1985, 83, 1010.

⁽¹⁹⁾ Hase, W. L. In ref 5.

TABLE VI: Values of k_{∞}^{II} (Minimization at Each E)

	(·····································		
temp, K	N	$k_{\infty}^{\text{II}} \pm \delta$, $10^{13} \text{ cm}^3 \text{ mol}^{-1} \text{ s}^{-1}$	
	$\alpha = 1.0 \text{ Å}^{-1}$		
300	6	4.28 ± 0.10	
	10	4.19 ± 0.08	
500	6	3.58 ± 0.08	
1000	6	2.29 ± 0.06	
2000	6	1.08 ± 0.03	
	10	1.08 ± 0.03	
	$\alpha = 0.8 \text{ Å}^{-1}$		
300	6	3.68 ± 0.08	
500	6	3.11 ± 0.07	
1000	6	1.99 ± 0.04	
2000	6	0.95 ± 0.03	

 aN denotes the number of i points in the sum of eq IV.3; $k_{\infty}^{\rm II}=\frac{1}{2}[(k_{\infty}^{\rm II})_{\rm max}+(k_{\infty}^{\rm II})_{\rm min}]$ and $\delta=\frac{1}{2}[(k_{\infty}^{\rm II})_{\rm max}-(k_{\infty}^{\rm II})_{\rm min}]$, where $(k_{\infty}^{\rm II})_{\rm max}$ and $(k_{\infty}^{\rm II})_{\rm min}$ are estimated upper and lower bound obtained by using $N_{E_i}+\sigma^{\rm MC}$ and $N_{E_i}-\sigma^{\rm MC}$, respectively, in eq IV.3.

The choice $\alpha=1.0$ Å⁻¹ for the interpolation parameter α in eq III.3, although reasonable, is somewhat arbitrary and for comparison calculations at T=300 and 2000 K were made by using $\alpha=0.8$ Å⁻¹ in V_1 (eq III.4). The resulting k_{∞}^{-1} values are given in Table IV. At both the high (2000 K) and low (300 K) temperatures the calculated rate constant decreased about 10% when α was changed from 1.0 to 0.8 Å⁻¹. Some decrease was expected since a smaller α tends to decrease $N_{E,I_k}(R)$ values when R is not too large. For each (E_i, J_k) pair in eq IV.1 the transition-state location R_1^{\dagger} is found to depend weakly or not at all on the values of α considered here. (Some R_1^{\dagger} results are given in Table V, although only for $\alpha=1.0$ Å⁻¹.)

The dependence of the transition-state location, as well as the sums of states at the transition state and at large radical separations $(R = \infty)$, on energy and angular momentum is illustrated in Table V, which gives values of R_1^{\dagger} , $N_{EJ}(R_1^{\dagger})$, and the ratio $N_{EJ}(R_1^{\dagger})/N_{EJ}(\infty)$, for various J's (0 to 100) and E's. These E's were chosen from the set of 24 Laguerre quadrature points E_i as determined by using N = 6 for each of the four temperatures. The transition-state location R_1^{\dagger} is almost independent of J for $E - E_{2p} \ge 2$ kcal mol⁻¹ (Table V). For $E - E_{2p}$ less than 2 kcal mol⁻¹, R_1^{\dagger} decreases rapidly with increasing J (Table V), but for a given (E, J) pair the associated N_{EJ} values vary only slowly with R. These observations suggest that the k_{∞}^{Π} value should provide a good approximation to that of the rigorous k_{∞}^{Π} , a result confirmed below. At a given energy $N_{EJ}(R_1^{\dagger})$ itself, incidentally, can vary with J over 1–2 orders of magnitude in the range J = 0–100.

The ratio $N_{EJ}/N_{EJ}(\infty)$ in Table V is seen to be a strongly decreasing function of both E and J, approaching unity at low $E - E_{zp}$ (≤ 2 kcal mol⁻¹) and low J (≤ 25) and approaching zero at high $E - E_{zp}$ and high J. This finding indicates that, for the present model system, a loose transition-state model with $N_{EJ}/N_{EJ}(\infty) \sim 1$ for all E and J is inapplicable.

Results for the k_{∞}^{11} rate constant are given in Table VI and are seen to agree with the k_{∞}^{I} values of Table IV, within the estimated Monte Carlo errors. In the calculation of k_{∞}^{II} there is a significant saving in computation time over that of k_{∞}^{I} . The inclusion of the J integration in the phase-space integral increases the dimensionality of the Monte Carlo problem by one and, hence, increases the associated variance for a given number of Monte Carlo points. It was found that, for each R value, using twice as many points to calculate $N_{E_i}(R)$ as to calculate $N_{E_iJ_k}(R)$ yielded comparable Monte Carlo variances for these two quantities. The elimination of individual Monte Carlo calculations for each of the discrete J_k in eq IV.1 values more than compensated for this increase and reduced the total number of Monte Carlo points required to obtain k_{∞}^{II} by factors of about 3, 4, 4, and 5 for T = 300, 500, 1000, and 2000 K, respectively. The present results, of course, have only established the agreement of k_{∞}^{II} and k_{∞}^{I} for the particular model system under study.

We also explored "canonically" calculated k_{∞} 's, denoted by k_{∞}^{III} , which are given in Table VII together with the corresponding transition-state locations R_{III}^{\dagger} . The k_{∞}^{III} values are seen to be

TABLE VII: Values of k_{∞}^{III} (Minimization at Each T)^a

temp, K	R_{III}^{\dagger} , Å	$k_{\infty}^{\text{III},b} 10^{13} \text{ cm}^3 \text{ mol}^{-1} \text{ s}$		
300	4.2	5.08 ± 0.13		
500	3.8	4.38 ± 0.06		
1000	3.4	2.79 ± 0.06		
2000	3.0	1.32 ± 0.03		

 $^a \alpha = 1.0 \text{ Å}^{-1}$. $^b k_\omega^{\text{III}} = ^1/_2[(k_\omega^{\text{III}})_{\text{max}} + (k_\omega^{\text{III}})_{\text{min}}]$ and $\delta = ^1/_2-([k_\omega^{\text{III}})_{\text{max}} - (k_\omega^{\text{III}})_{\text{min}}]$, where $(k_\omega^{\text{III}})_{\text{max}}$ and $(k_\omega^{\text{III}})_{\text{min}}$ are estimated upper and lower bounds obtained by using $N_{E_l} + \sigma^{\text{MC}}$ and $N_{E_l} - \sigma^{\text{MC}}$, respectively, in eq IV.4.

TABLE VIII: Values of k_{∞} 's with Approximate Symmetry Correction^a

temp, K	$k_{\infty}^{1'} \pm \delta,^{b}$ 10 ¹³ cm ³ mol ⁻¹ s ⁻¹	$k_{\infty}^{II'} \pm \delta_{,c}^{c} 10^{13}$ cm ³ mol ⁻¹ s ⁻¹
300	4.31 ± 0.10	4.31 ± 0.10
500		3.64 ± 0.08
1000		2.52 ± 0.06
2000	1.53 ± 0.05	1.49 ± 0.04

 $^{a}\alpha=1.0~\text{Å}^{-1}.~^{b}k_{\omega}^{~^{I}}$ and δ are determined as in the footnote of Table IV but with $N_{E_{i}I_{k}}$ replaced by $N_{E_{k}I_{b}'}$. See section IV.i for details. $^{c}k_{\omega}^{~^{II}}$ and δ are determined as in the footnote of Table VI but with $N_{E_{i}}$ replaced by $N_{E_{i}'}$. See section IV.ii for details.

greater than the corresponding k_{∞}^{I} or k_{∞}^{II} values (see Tables IV and VI) by a factor of about 1.2 for all four temperatures studied. Since at each R, $N_{EJ}(R) \ge N_{EJ}(R^{\dagger})$, it is clear that k_{∞}^{III} should be an upper bound to k_{∞}^{I} . Indeed, one can show that $k_{\infty}^{III} \ge k_{\infty}^{II} \ge k_{\infty}^{II}$.

There also proved to be no computational advantage in calculating k_{∞}^{III} for the present model. Attempting to remove the energy quadrature in eq IV.4 by including the energy integral in a straightforward way in the present Monte Carlo procedure substantially increased the standard deviation σ^{MC} . Reducing σ^{MC} to an acceptable value would have required extra computer time, or modifying the Monte Carlo method, and the computational effort expended to obtain k_{∞}^{III} via the energy quadrature was approximately the same as that required for the preferred k_{∞}^{II} for the present treatment of this system.

It can also be seen in Table IV that when the number of quadrature points was varied the $k_{\infty}^{\rm I}$ values so obtained agreed within the uncertainty imposed by the Monte Carlo procedure. The other calculations of $k_{\infty}^{\rm I}$ in Tables IV and VII were therefore performed with N=6 and $\Delta J=25$. The convergence of the Laguerre quadrature over E was also checked for T=300 and 2000 K by comparing $k_{\infty}^{\rm II}$ values obtained from eq IV.3 with N=6 and 10. For both temperatures the excellent agreement justified the use of the six-point quadrature for the remaining results for $k_{\infty}^{\rm II}$ and $k_{\infty}^{\rm III}$ (Tables VII–IX).

To consider the effect of the symmetry correction proposed in footnote 16, results are given for $k_{\infty}^{\ \ I'}$ and $k_{\infty}^{\ \ II'}$ in Table VIII. The transition-state location $R_{\rm I}^{\ \ I'}$ (or $R_{\rm II}^{\ \ I'}$) is that value of R (in infinite transition). crements of 0.1 Å⁻¹) which minimizes the N_{E,J_k} (or N_{E_i}), defined in footnote 16, for given E_i and J_k (or E_i) and is, in general, not equal to R_{I}^{\dagger} (or R_{II}^{\dagger}). No additional computations are required to obtain the N_{E,I_k}^{Λ} appearing in footnote 16. During the Monte Carlo evaluation of $N_{E,J_k} = N_{E,J_k}^A + N_{E,J_k}^B + N_{E,J_k}^C$ one simply identifies the subset of randomly selected configurations corresponding to A and processes the data for N_{E,J_k} and N_{E,J_k}^{A} in parallel; an analogous procedure is followed for the k_{∞}^{II} calculation. At T = 300 and 2000 K, the $k_{\infty}^{I'}$ and $k_{\omega}^{II'}$ values agree to within the Monte Carlo uncertainty as did the corresponding k_{∞}^{-1} and k_{∞}^{II} . Further discussion is therefore confined to the more readily evaluated k_{∞}^{II} rate constants. At T = 300 and 500 K, $k_{\infty}^{II'}$ agrees with corresponding k_{∞}^{II} in Table VII to within the Monte Carlo uncertainty. At T = 1000 K, $k_{\infty}^{\text{II}'}$ is about 10% greater than k_{∞}^{II} ; at T = 2000 K the same relationship is observed but the relative difference has increased to about 40%. In terms of the present model this trend is attributable to the decrease in $R_{\rm H}^{\dagger}$ with the increase in the available energy E associated with increasing temperature. Table V illustrates this point for R_1^{\dagger} , and the sit-

TABLE IX: Comparison of N_E and N_E^A as a Function of R at E - $E_{zp} = 63.52 \text{ kcal mol}^{-1}$

R, Å	$[N_E \pm \sigma^{\rm MC}]/10^{18}$	$[N_E^A \pm \sigma_A^{MC}]/10^{18}$	ρ
2.2	0.597 ± 0.037	0.597 ± 0.037 -	1.00
2.3	0.473 ± 0.026	0.469 ± 0.026	0.99
2.4	0.357 ± 0.016	0.343 ± 0.016	0.96
2.5	0.298 ± 0.012	0.261 ± 0.012	0.88
2.6	0.299 ± 0.010	0.231 ± 0.009	0.77
2.7	0.323 ± 0.008	0.218 ± 0.007	0.67
2.8	0.360 ± 0.007	0.201 ± 0.006	0.56
2.9	0.453 ± 0.007	0.219 ± 0.006	0.48
3.0	0.563 ± 0.008	0.235 ± 0.005	0.42
3.1	0.773 ± 0.009	0.289 ± 0.006	0.37
3.2	1.01 ± 0.01	0.342 ± 0.006	0.34
3.4	1.72 ± 0.02	0.528 ± 0.010	0.31
100	29.4 ± 0.5	7.63 ± 0.24	0.26

the "effective" or "collective" transition state for T = 300 and 500 K can be termed loose and is seen to become tighter as T is increased beyond 500 K. The effect of the potential surface V_i on the energetically allowed configuration types with decreasing R and the need for the symmetry correction are illustrated in Table IX. The energy under consideration is $E - E_{zp} = 63.52 \text{ kcal mol}^{-1}$. the value of E_6 in the N=6 Laguerre quadrature at T=2000K. Given are the Monte Carlo estimates N_E and N_E^A and their associated standard deviations for the cited R values; also given is the ratio $\rho = N_E^A/N_E$. It may be noted that at R = 2.2 Å, the smallest R value considered in any of the present calculations, ρ equals 1.0 and that as R increases ρ tends to $^{1}/_{4}$, as expected. In addition, $R_{\rm II}^{\dagger}$ (= 2.5–2.6 Å) is less than $R_{\rm II}^{\dagger'}$ (= 2.8 Å) at this (high) energy.

uation for $R_{\rm II}^{\dagger}$ is no different. Based on the $k_{\infty}^{\rm II}$ and $k_{\infty}^{\rm II'}$ results,

VI. Comparison of k ... with Experiment and Other Calculations

In this section the results for k_{∞} are first compared with the available experimental data. The features of several earlier theoretical treatments of methyl radical recombination, each of which led to a different prediction for the magnitude and temperature dependence of k_{∞} , are then described. The following discussion focuses heavily on Figure 2, a semilog plot of k_{∞} vs.

Experimental values for the high-pressure methyl radical recombination rate constant are indicated by the various symbols in Figure 2; the associated references are listed in the figure caption. For pictorial clarity the associated experimental uncertainties are not depicted in Figure 2. Those values of k_{∞} obtained by conversion of a measured unimolecular rate constant for ethane decomposition by using an equilibrium constant are so identified in the figure caption. A comprehensive review of pre-1980 experimental work on methyl radical recombination was published by Baulch and Duxbury.20 All of the pre-1978 citations in the present paper (ref 28-46) but one (ref 42) can be found in their Table 1 along with the experimental method and, in most cases, the experimental uncertainty. Their Table 1 is extensive and, to avoid considerable congestion and overlapping of symbols, particularly at $T \approx 300$ K, no attempt was made to include all the entries therein in Figure 2. While many of the 1979-1985 experimental citations (ref 21-27) were obtained by a literature search, the list may not be exhaustive. For experimental details and estimated uncertainties of the 1979-1985 work the reader is referred to the individual references.

Despite the scatter and uncertainty in some of the measured data, the currently available experimental k_{∞} values have been regarded by various authors as displaying a negative temperature dependence; i.e., k_{∞} decreases as T increases. 21,26 For example, the center of gravity of points at 300 K is higher than that at 1400 K by a factor of about 3. However, accurate experimental de-

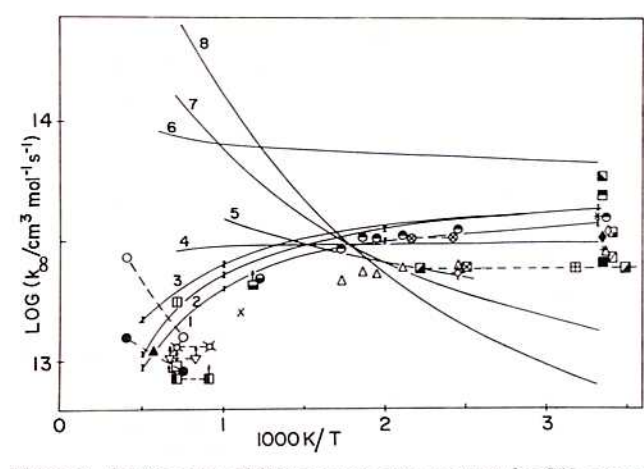


Figure 2. Semilog plot of high-pressure rate constant for CH3 recombination vs. reciprocal temperature. Theoretical results are presented as the solid curves labeled 1-8 and are discussed in the text. Experimental results are plotted as symbols. Identical symbols connected by a dashed line indicate that the reported rate spans a temperature range; a lower bound on a measured rate is indicated by an upward pointing arrow on top of the symbol. In the following list, results obtained from kinetic studies involving CH3 recombination are identified by a symbol alone and those obtained by conversion of measured C2H6 dissociation rates by a symbol and a "d": (♠) ref 21; (△) ref 22; (+) ref 23; (♦) ref 24; (▲) ref 24; (0, d) ref 25; (0, d) ref 26; (0) ref 27; (0) ref 28; (11) ref 29; (♥) ref 30; (□) ref 31; (□) ref 32; (□, d) ref 33; (□) ref 34; (□) ref 35; (□, d) ref 36; (□) ref 37; (♥) ref 38; (■) ref 39; (□) ref 40; (□) ref 41; (⊗) ref 42; (×, d) ref 26, 43; (♦) ref 44; (*) ref 45; (⋈) ref 46.

terminations of high-pressure recombination rate constants at high temperature require an extrapolation of the results at various pressures, and consequently there is clearly uncertainty in the quantitative temperature dependence of k_{∞} at high temperatures, where a large extrapolation is needed.

The collective data are seen to be in qualitative agreement with the present treatment as represented by curves 1-3 in Figure 2. Because of the scatter, the significance of this agreement at high temperatures, as well as the applicability of the particular statistical model described herein, will require more accurate experimental data in the 1000-2000 K range. Curves 1 and 2 depict k_{∞}^{II} for $\alpha = 0.8$ and 1.0 Å⁻¹, respectively, and curve 3 depicts $k_{\infty}^{II'}$ for $\alpha = 1.0 \text{ Å}^{-1}$, each curve being obtained by smoothly connecting the calculated values of k_{∞} at T = 300, 500, 1000, and 2000 K.At each of these temperatures the estimated Monte Carlo uncertainty in the k_{∞} values is indicated by error bars whose range corresponds to the upper and lower bounds as given in the appropriate table. Of interest is the excellent quantitative agreement between the recently published data of Macpherson, Pilling, and Smith²¹ and the present calculations for the experimentally studied temperature range 296-577 K. In Figure 2 it can be seen that their data, as represented by circles with solid upper half, are close to curves 1 and 2 over this temperature range. The significance of the data in ref 21 is the accurate determination of the absorption cross section σ for the CH₃ transition at 216.36 nm described therein. Since most experimental studies of methyl radical recombination employ optical detection of CH₃ at this wavelength and accurately measure k_{∞}/σ , an accurate measurement of σ over the temperature range of interest must be performed to determine the T dependence of k_{∞} . In many earlier determinations of k_{∞} a major source of error appears to lie in the absorption cross section, a case in point being the earlier work of Macpherson, Pilling, and Smith,22 represented by the open triangles in Figure

⁽²⁰⁾ Baulch, D. L.; Duxbury, J. Combust. Flame 1980, 37, 313.

⁽²¹⁾ Macpherson, M. T.; Pilling, M. J.; Smith, M. J. C. J. Phys. Chem. 1985, 89, 2268.

⁽²²⁾ Macpherson, M. T.; Pilling, M. J.; Smith, M. J. C. Chem. Phys. Lett. 1983, 94, 430.

⁽²³⁾ Laguna, G. A.; Baughcum, S. L. Chem. Phys. Lett. 1982, 88, 568. (24) Adachi, H.; Basco, N.; James, D. G. L. Int. J. Chem. Kinet. 1980,

⁽²⁵⁾ Zaslonko, I. S.; Smirnov, V. N. Fiz.-Khim. Protesessy Gazov. Kondens. Fazakh 1979, 19 (in Russian). Kinet. Katal. 1979, 20, 575 (in Russian). (26) Olson, D. B.; Gardiner, W. C. J. Phys. Chem. 1979, 83, 922. (27) Pacey, P. D.; Wimalasena, J. H. J. Phys. Chem. 1980, 84, 2221.

2, in which the same k_{∞}/σ ratios were employed as in ref 21. Also depicted in Figure 2, as curves 4-8, are the k_{∞} predictions

of several other theoretical treatments. Curve 4 displays a very small negative temperature dependence and is obtained from

calculations³⁰ based on the statistical adiabatic channel model (SACM) of Quack and Troe.8 It spans the temperature range 300-1350 K. Details of this model are given in ref 8; the salient

features of the SACM and a numerical comparison between it and our model for N_{EJ} in the dissociation of NO_2 were described

in part 2. The utility of the present method is emphasized, in part, by examining the relative computational effort involved in applying

it and SACM (and, in part, by noting that given a potential energy surface it has no adjustable parameters). In part 2 it was found

for the NO2 system that the present model was computationally faster for the evaluation of N_{EJ} for the larger values of E and J. Although no SACM computations were performed by us for the $C_2H_6 \leftrightarrow 2CH_3$ system, it is apparent that the greater number of atoms will drastically increase the number of reactant and product energy levels to be correlated, especially at higher temperatures where the average values of E_{∞} and J are larger. In their SACM treatment of C₂H₆ dissociation, Quack and Troe found it necessary to correlate "states of individual (transitional) coordinates

separately...(to avoid) the complex six-dimensional correlation problem", presumably to obtain a computationally tractable model. Subsequent work⁴⁷ on the SACM has focused on the introduction of approximations which reduce, relative to the original version,8 the computational effort in applying this model. Cobos and Troe¹⁸ have recently summarized a two-parameter canonical version of the SACM and applied it to a number of association reactions. In curve 5 the high-pressure methyl radical recombination rate

constant for the range 400-1000 K, predicted by Hase's treatment of this system, ¹⁹ is given. It shows a positive temperature dependence of k_{∞} . In Hase's work a density of states $N(r_{\rm CC})$ was obtained (by exact count or semiclassically) as a function of the available internal energy and external rotational energy by treating the critical configuration as a collection of rigid rotors and harmonic oscillators with several additional approximations.⁴⁸ Hase's critical configuration was chosen as that value of r_{CC} which minimized the density of states N(r_{CC}) in the hypersurface orthogonal to r_{CC} . Both the canonical (activated complex) and the more detailed microcanonical (RRKM) minimizations of this state density were performed and found to be in good agreement with each other (after integrating the microcanonical results over the Boltzmann distribution of energy); the canonical results (the counterpart of k_{∞}^{III} in our notation) reported in Table IV of ref

19 were used to construct curve 5.

It is also of interest to compare the theoretical and experimental results to a rate $k_{\rm coll}$ based on a Gorin-type collision theory.⁴⁹ Curve 6 in Figure 2 is a plot of $k_{\rm coll} = 1/2g_{\rm e} \langle Z_{\rm coll} \rangle$ over the 300-2000 K temperature range. Here g_e is the ratio of electronic partition functions as discussed in section I and $\langle Z_{coll} \rangle$ is a Boltzmann average of the collision frequency as obtained from a Gorin model in which the two methyl radicals are treated as point masses moving under the influence of a central potential.50 The collision frequency⁵⁰ is

$$\langle Z_{\text{coll}} \rangle = \frac{2.25\pi R_e^2}{(\mu/2)^{1/2}} (D_{\text{CC}})^{1/3} (kT)^{1/6} (1.02)$$
 (VI.1)
The parameters R_e and D_{CC} are listed in Table III. This model,

which has an explicit positive temperature dependence of $T^{1/6}$, was intended in ref 50 only to provide an estimate of an upper bound for the recombination rate and a basis for the discussion and calculation of steric factors. Curves 7 and 8 depict RRKM-type treatments of the recombination rate in which no minimization of the sum over states or

density of states for the critical configuration was attempted and in which the coordinates in the transition state were again approximated as free rotors and harmonic oscillators. The calculations of Waage and Rabinovitch30,51 (curve 7) and Quack and Troe^{8,30} (curve 8) are essentially the same. The salient features of the Waage-Rabinovitch treatment of the critical configuration^{27,51} and given in footnote 52, together with minor differences of the Quack-Troe treatment. Not displayed in Figure 2 but worth discussing are several unsuccessful attempts by Olson and Gardiner26 to improve one

RRKM treatment, as embodied in curves 7 and 8, so as to bring theory and experiment into better agreement. Their first approach was a straightforward modification of the Waage-Rabinovitch

calculation. A direct count of vibrational states was introduced for energies less than 12 kcal mol-1 above threshold, and the semiclassical formula was retained for higher energies. In addition, the torsional motion of the CH₃ groups at the critical configuration was treated as a hindered rotor instead of a free rotation and a direct counting procedure was used to include these hindered rotor energy levels in the sum of states. The resulting k vs. 1/T curve, labeled RRKM in Figure 2 of ref 26, is seen to be qualitatively the same as curves 7 and 8 in the present Figure 2. In their second approach Olson and Gardiner performed calculations similar to those of Hase, 19 described earlier. The critical configuration was chosen by a minimum state density criterion. A Morse function was used for the C-C potential curve; the degenerate CH3 moments of inertia were modeled to increase as the square of the

reaction coordinate r_{CC} , and the third moment was taken as constant; the CH₃ rocking frequencies in C₂H₆ were assumed to

decrease exponentially with r_{CC} as $g(r_{CC})$; the same exponential

decay was used to describe the fundamental torsional frequency

which determined the barrier to internal rotation. The interpo-

⁽²⁸⁾ Callear, A. B.; Metcalfe, M. P. Chem. Phys. 1976, 14, 275. (29) Glanzer, K.; Quack, M.; Troe, J. Symp. (Int.) Combust., [Proc.], 16th, 1976 1977, 949. (30) Glanzer, K.; Quack, M.; Troe, J. Chem. Phys. Lett. 1976, 39, 304. (31) Parkes, D. A.; Paul, D. M.; Quinn, C. P. J. Chem. Soc., Faraday

Trans. 1 1976, 72, 1935. (32) Clark, J. A.; Quinn, C. P. J. Chem. Soc., Faraday Trans. 1 1976, 72,

^{706.} (33) James, F. C.; Simons, J. P. Int. J. Chem. Kinet. 1974, 6, 887.

⁽³⁴⁾ Bass, A. M.; Laufer, A. H. Int. J. Chem. Kinet. 1973, 5, 1053. (35) Truby, F. K.; Rice, J. K. Int. J. Chem. Kinet. 1973, 5, 721.

⁽³⁶⁾ Burcat, A.; Skinner, G. B.; Crossley, R. W.; Scheller, K. Int. J. Chem.

Kinet. 1973, 5, 345.

⁽³⁷⁾ Clark, T. C.; Izod, T. P. J.; Kistiakowsky, G. B. J. Chem. Phys. 1971,

^{54, 1295.} (38) Clark, T. C.; Izod, T. P. J.; Di Valentin, M. A.; Dove, J. E. J. Chem.

Phys. 1970, 53, 2982. (39) Basco, N.; James, D. G. L.; Stuart, R. D. Int. J. Chem. Kinet. 1970,

⁽⁴⁰⁾ Braun, W.; Bass, A. M.; Pilling, M. J. Chem. Phys. 1970, 52, 5131.

⁽⁴¹⁾ Van Den Berg, H. E.; Callear, A. B.; Norstrom, R. J. Chem. Phys. Lett. 1969, 4, 101. Van Den Berg, H. E. Dissertation, Cambridge, UK, 1971.

⁽⁴²⁾ Biordi, J. C. Melon Inst. Radiat. Res. Lab. Q. Rep. 1969, 47, 12. (43) Lin, M. C.; Back, M. H. Can. J. Chem. 1966, 44, 2357

⁽⁴⁴⁾ March, R. E.; Polanyi, J. C. Proc. R. Soc. London, A 1963, 273, 360. (45) Moseley, F.; Robb, J. C. Proc. R. Soc. London, A 1957, 243, 130.

⁽⁴⁶⁾ Gomer, R.; Kistiakowsky, G. B. J. Chem. Phys. 1951, 19, 985.

⁽⁴⁷⁾ Troe, J. J. Chem. Phys. 1981, 75, 226; 1984, 79, 6017. (48) The two degenerate CH₃ rocking frequencies, which are termed

transitional modes in our treatment, were assumed to have rcc-dependent frequencies given by $\omega g(r_{CC})$, where ω is the rocking frequency in C_2H_6 and $g(r_{CC})$ is eq III.3 with R and R_c replaced by r_{CC} and $r_{CC,c}$. The interpolation parameter α in the expression for g was selected to be 0.82 Å⁻¹ by fitting a calculated C2H6 rate constant to one measured in a chemical activation experiment. In addition, r_{CC} -dependent moments of inertia were employed to determine rotational energies, a Morse function was chosen to model the reaction coordinate potential, and it was assumed that internal rotation becomes a free rotor for $r_{\rm CC} > 2.6$ Å. Explicit conservation of the total angular momentum J was not included in this model.

⁽⁴⁹⁾ Gorin, E. J. Chem. Phys. 1939, 7, 256, 633. (50) Benson, S. W. In ref 5. Equation VI.1 includes the factor of πR_e^2

which was accidentally omitted from his eq 11.
(51) Waage, E. V.; Rabinovitch, B. S. Int. J. Chem. Kinet. 1971, 3, 105.

⁽⁵²⁾ The cc was fixed at an r_{CC} distance of 2.7 Å, and the moment of inertia of the cc was assumed to be 2.45 times the C_2H_6 value. The torsional

vibration of C2H6 was assumed to have become a free rotor, and the two from 822 and 1190 cm⁻¹, respectively, in C_2H_6 . The sum of states at the cc was evaluated by using a semiclassical formula. In the Quack-Troe treatment the dissociation energy of the C-C bond in C_2H_6 was taken as $D_0(C-C) = 87.76$ kcal mol⁻¹, instead of the 86.3 kcal mol⁻¹ used by Waage and Rappoints. novitch. Other differences between the two treatments are presumably minor; details of the Quack-Troe calculation are omitted in ref 8.

rotated axis y

 $\mathbf{j}_1 \times \mathbf{j}_2 = \mathbf{j}_1 \times \mathbf{k}$

 $\kappa_i \times \mathbf{j}_i$

TABLE X: Definition of Angles Used in Rotational Transformations (a) Conjugate Angles^a angular conjugate momentum angle

angular

axis x $1 \times j_2$ k $1 \times k$ α_{ν} $1 \times j_i$ j_i α_i $\kappa_i \times \mathbf{j}_i^d$ γ_i $1 \times j_2^b$ j_{1z}

(b) Contained Angles

momentum раіг angle χ $\overline{(J^2-l^2-k^2)/2lk}$ θ_{lk} (l, k) $\frac{(k^2 - j_1^2 - j_2^2)/2j_1j_2}{(j_1^2 + k^2 - j_m^2)/2j_1k} (i = 1, 2; m = 2, 1)$ θ_{12} (j_1, j_2) (k, j_i) θ_{ki} $(\cos \theta_{lk} \cos \theta_{ki} + \sigma \sin \theta_{lk} \sin \theta_{ki} \cos \alpha_k (i = 1,$ (l, j_i) 2; $\sigma = +1, -1$) $\kappa_i/j_i^d \ (i=1,\,2)$ (j_i, κ_i) ^a All conjugate angles range from 0 to 2π and are obtained by

counterclockwise rotation about $x \times y$ from x to y. The subscript i

refers to fragment 1 or 2. ^bCorresponds to axis x in Figure 1a.

^c Corresponds to line of nodes N_1 in Figure 1a. ^d Corresponds to line of

nodes N_1''' in Figure 1a for i = 1. In all cases $0 \le \theta \le \pi$ and $\sin \theta$ is

obtained from $\cos \theta$ as the positive root. the minimization is made only after summing over J and integrating over E. However, in the calculation of k_{ω}^{III} extending the present Monte Carlo method to include the integral over E, thereby removing the apparently more laborious energy quadrature in eq IV.4, offered no computational advantage, although other Monte Carlo methods may do so.

In the calculation of the number of states, N_{EJ} , an approximation was introduced (described in footnote 16) for the treatment of the out-of-plane inversion motion of the CH₃'s which led to the calculation of other constants k_{∞}' for comparison with k_{∞} . This approximation can be removed by a more elaborate quantum treatment of that coordinate, in the presence of the other coordinates. We plan to treat this aspect in a later paper. Some measure of the effect is roughly inferred by comparing the values of k_{∞} and k_{∞}' . They approximately agree at the lower temperatures and differ by about 40% at the highest temperature.

The present calculations are based directly on some knowledge of the potential energy surface. They serve, thereby, to identify those parts of the surface which determine the value of k_{∞} . Since k_{∞}^{III} provides a reasonable yet "consolidated" approximation to k_{∞}^{I} , its calculation can be used to determine the important region $(R = R_{III}^{\dagger})$ of the surface. The region depends on the temperature, as one sees from Table VII; namely, the R^{\dagger} values range from about 3.0 Å at 2000 K to about 4.2 Å at 300 K. At 4.2 Å, almost all mutual orientations of the methyl radicals made a significant contribution to N_{EJ} , whereas at 3.0 Å those orientations corresponding to configuration A (the CH₃ umbrellas opening away from each other; see section III) dominated. Since only a limited number of points of the potential energy surface can be obtained in practice with quantum chemistry calculations, it will be desirable to "spline" the points so determined by using some functional form for the dependence on the angular coordinates. One possible form is that used in Appendix B (present parameters in Table XI), but some other form may be better. In such calculations of the potential energy surface the force constants of the "conserved" vibrations in this region can also be determined and thereby the use of the parameter α in eq III.3 avoided.

Among the features of the present method which may be mentioned are the following: 1. It includes full angular momentum conservation.

- 2. It proceeds directly from the potential energy surfaces themselves rather than assuming some parametrization of the energy levels. In this way it is associated with a fundamental implementation of the statistical model. (The interpolation and the α in eq III.3 can be avoided, as already noted, when an improved potential energy surface becomes available.)
- of about 20%, values of k_{∞}^{III} could also have been used, in which (53) Growcock, F. B.; Hase, W. L.; Simons, J. W. Int. J. Chem. Kinet.
- (54) Two separate computer programs were used in the present numerical treatment. The determination of R-dependent potential parameters, the analysis of the V_t potential (section III and Appendix C), and the least-squares fitting of Morse parameters for the bond-fission potential were done by a preliminary program. The resulting data were stored, according to the R value, and used repetitively by a main program dedicated to the evaluation
- of N_{EJ} (or N_E). The largest single section of the main program simply initializes, controls, and summarizes the Monte Carlo procedure. The following repetitively executed processes form the core of the Monte Carlo calculation and are not difficult to program: the selection of a multidimensional point in action-angle space (in which step angular momentum and energy conservation are ensured), the transformation from action angle to internal coordinates, and the evaluation of the transitional mode potential. These steps involve about 70, 120, and 40 lines of FORTRAN code, respec-

tively. The evaluation of the sum of conserved vibrational states N_V is done

once for each R value and is described in part 2.

their RRKM treatment and experiment, the authors of ref 26

modified their second approach as follows: The two doubly de-

generate CH₃ rocking modes were treated as four independent

hindered rotations, and a direct count of the associated energy

levels plus those of the hindered torsional motion was performed

in the sum of state calculation. The restricting barriers of all five

hindered rotations were reduced exponentially with increasing r_{CC} .

Using the interpolation parameter of $\alpha = 0.75 \text{ Å}^{-1}$, one obtains

the curve labeled BPHR in Figure 2 of ref 26. Although it

predicted a smaller temperature dependence than the BPV model

(discussed above) with loosened CH₃ rocking vibrations, the

authors determined the decomposition rate constant for vibra-

tionally excited ethane produced by chemical activation, $C_2H_6^*$ \rightarrow 2CH₃. The reported⁵³ excitation energy of 114.9 \pm 2 kcal mol⁻¹

with respect to the zero-point energy of ethane corresponds, for

the present molecular parameters (Table XI), to an energy of 27.3

± 2 kcal mol⁻¹ with respect to the zero-point energy of separated

methyl radicals. Here we assume that this excitation energy is

deposited in internal degrees of freedom and that the overall rotational energy of ethane is approximated by $E_J = J(J+1)/2I_{A,r}$

(in units of h = 1) with a symmetric top moment of inertia $I_{A,r}$

defined in part 2. For J-dependent total energies $E - E_{zp} = 27.3$

+ E_J and various J's, $N_{EJ}(R_I^{\dagger})$ was determined as described in section IV.i. In each case R_I^{\dagger} was found to be 2.9 ± 0.1 Å. Rate

constants $k_{EJ} = N_{EJ}(R_I^{\dagger})/h\rho_{EJ}$, where ρ_{EJ} is a state density for

ethane obtained via the method described in part 2, were then

calculated. The results are as follows: k_{EJ} (in 10^9 s⁻¹) = 4.6, 4.2,

4.4, 6.9, 14, and 33 for J = 0-125 in increments of 25. These

calculated k_{EJ} values agree, for $J \lesssim 75$, with the reported⁵³ ex-

perimental value of $(4.6 \pm 1.2) \times 10^9$ s⁻¹. The experimental J

distribution is not known. If J had its thermally averaged value

at room temperature (the temperature in the photolysis experi-

ment⁵³ was not specified, however), then the average J would be

about 25. In any event a J distribution in which the dominant

The present results show that the negative temperature de-

pendence reported (Figure 2) for the extrapolated high-pressure

rate constants k_{∞} for methyl radical recombination can be un-

derstood in terms of deviation from a loose transition state. At

the present time the theory and experiment for k_{∞} are in agree-

ment, but further experimental data are needed. We have also

seen that k_{∞}^{II} , in which one first sums over J in eq I.3 before

minimizing with respect to R at each E, provides an excellent

approximation to k_{∞}^{-1} , in which the minimization is performed for

each E and J (Tables IV and VI). The saving in computational

time was about a factor of 4 on the average. With an added error

 \mathcal{F} s are less than 75 is likely.

1973, 5, 77.

VII. Discussion and Summary

Another test of the present model for N_{EJ} is afforded by the

agreement with the experimental data remained poor.

experimental data of Growcock, Hase, and Simons.⁵³

lation parameter α in $g(r_{CC})$ was varied widely, and the optimum result is labeled as curve BPV in Figure 2 of ref 26. The agreement with the experimental data is not good and was not better for other values of α . In a final attempt to rectify the disagreement between

(A.3)

(B.2)

The Journal of Physical Chemistry, Vol. 90, No. 21, 1986

TABLE XI: Potential Parameters for the CH₁...CH₁ System

IADLE AI: FOTEIILIA	i raiameteis	IUI LI	ie Cii3Cii3 Syste	3111	
parameter	value	ref	parameter	value	ref
	C ₂	H ₆			
r _{CH,e} , Å	1.111	59	R_{e} , Å	1.696	a
r _{CC,e} , Å	1.533	59	$D_{\rm CC}$, kcal mol ⁻¹	96.6	b
α _{HCH,e} , deg	107.3	59	β_{CC} , $\mathring{\mathbf{A}}^{-1}$	1.80	с
$\beta_{HCC,e}$, deg	111.4	59	$D_{\rm CC}^{\rm ef}$, kcal mol ⁻¹	202.5	d
$\tau_{\rm e}$, deg	60	59	Recet A-1	1.90	d
$f_{\rm CC}$, erg cm ⁻²	4.342×10^{5}	60	$r_{\rm CC,e}^{\rm ef}$, Å	1.175	d
$D_0(C-C)$, kcal mol ⁻¹	87.60	59	00,0		
	CI	H,			
r _{CH,e} , Å	1.079	58	$\alpha_{\text{HCH,e}}$, deg	120	58
	CH ₃	·CH	1		
ε _{H⊶H} , kcal mol ⁻¹	0.010	57	r _{HH,0} , Å	3.37	57
ϵ _{CC} , kcal mol ⁻¹	0.095	57		3.88	57
koal mol-1	0.031	d	r Å	3.62	0

 ϵ_{C-H} , kcal mol

 $(\epsilon_{\text{C}...\text{H}}\epsilon_{\text{C}...\text{C}})^{1/2}$; $r_{\text{C}...\text{H},0} = \frac{1}{2}(r_{\text{H}...\text{H},0} + r_{\text{C}...\text{C},0})$.

of Canada (D.M.W.).

$$_{\text{H}}$$
, kcal mol⁻¹ 0.031 $d r_{\text{C-H,0}}$, Å 3.62 e

 C_2H_6 . $^bD_{CC} = D_0(C-C) + E_{zr} - E_{zp}$ where E_{zr} and E_{zp} are determined by the normal-mode frequencies of C_2H_6 and CH_3 , respectively, as listed in Tables I and II. $^c\beta_{CC} = (f_{CC}/2D_{CC})^{1/2}$. d Obtained by least-squares fitting as outlined in the text with $\alpha = 1.0$ Å⁻¹; slightly differ-

ent values of the parameters are obtained with $\alpha = 0.8 \text{ Å}^{-1}$. $\epsilon_{\text{C...H}} =$ 3. The method is easy to use and to program. There are some

initially tedious details involving the coordinate transformations, but they pose no fundamental difficulty. A brief outline of the computer programming involved in the present calculations is given in footnote 54. In the present paper attention has been focused on the high-

pressure rate constant for the methyl radical recombination reaction. The application of our results for N_{EJ} to the pressure dependence of this recombination will be discussed elsewhere.⁵⁵ Acknowledgment. It is a pleasure to acknowledge the support of this research by the National Science Foundation (R.A.M.) and by the Natural Sciences and Engineering Research Council

The internal coordinates r_{mn} , θ_1 , θ_2 in which the transitional mode potential is expressed are determined from the action-angle coordinates as follows. Atomic position vectors $\mathbf{r}_n^{(i)''}$ (n = 1, ...,

Appendix A. Action Angle and Internal Coordinates

4; i = 1, 2), as determined by the R-dependent CH₃ structure, are assigned in the fragment-fixed (x_i'', y_i'', z_i'') system and the separation vector \mathbf{R}''' is chosen to lie along the x''' axis of the triply primed (x''', y''', z''') system whose z''' axis lies along the z axis

of the molecule-fixed (x, y, z) system. By transforming each of R''', $\mathbf{r}_m^{(1)''}$, and $\mathbf{r}_n^{(2)''}$ to the (x, y, z) system, the coordinates $r_{mn} = |\mathbf{R} + \mathbf{r}_m^{(1)} - \mathbf{r}_m^{(2)}|$ (m, n = 1, ..., 4) and $\cos \theta_i = \mathbf{e}_{r_{CC}} \mathbf{e}_{z_i}^{"}$ (i = 1, 2) are readily obtained; here $r_{CC} = r_{44}$ and $\mathbf{e}_{z_i}^{"}$ specifies the symmetry axis of fragment i.

For given R, J, and 12-dimensional Monte Carlo point $(j_1, j_2, k, l, \kappa_1, \kappa_2, \alpha_1, \alpha_2, \alpha_k, \alpha_l, \gamma_1, \gamma_2)$ the vectors \mathbf{R} , $\mathbf{r}_m^{(1)}$, and $\mathbf{r}_n^{(2)}$ are obtained by application of the inverse rotation matrix \mathbf{A}^{-1} : $\mathbf{r}_{n}^{(i)} = \mathbf{A}^{-1}(\alpha_{i}, \theta_{li}, \beta_{i}) \ \mathbf{A}^{-1}(\gamma_{i}, \theta_{\kappa \rho}, 0) \mathbf{r}_{n}^{(i)''} \quad (i = 1, 2) \quad (A.1)$

$$\mathbf{R} = \mathbf{A}^{-1}(\alpha_h \mathbf{0}, \mathbf{0}) \mathbf{R}^{\prime\prime\prime} \tag{A.2}$$

$$\mathbf{R} = \mathbf{A}^{-1}(\alpha_i, 0, 0) \mathbf{R}^{-1}$$
 (A.2)
The first applications of \mathbf{A}^{-1} in eq A.1 yields the intermediate vector $\mathbf{r}_n^{(i)'}$ in the fragment-fixed (x_i', y_i', z_i') system which is rotationally

related to the (x_i'', y_i'', z_i'') system by the Euler angles $(\gamma_i, \theta_{\kappa_i}, \theta_{\kappa_i})$

0), where γ_i is conjugate to κ_i and θ_{κ_i} is the angle contained between κ_i and j_i (i.e., between the $z_i^{\prime\prime}$ axis and the $z_i^{\prime\prime}$ axis). The second set of Euler angles $(\alpha_i, \theta_{li}, \beta_i)$ in eq A.1 connect the (x_i', y_i', z_i') (55) Gutman, D.; Wagner, A. F.; Wardlaw, D. M., to be published. (56) Warshel, A. In Semiempirical Methods of Electronic Structure Calculation, Part A; Segal, G. A., Ed.; Plenum: New York, 1977.

(57) Goddard, W. A., private communication.

(58) Herzberg, G. Electronic Spectra of Polyatomic Molecules; Van Nostrand: New York, 1967.

set A in Table VII).

and (x, y, z) systems; α_i is conjugate to j_i , θ_{ii} is the angle contained between j_i and l (i.e., between the z_i' axis and the z axis), and β_i is the angle between the x axis and the x_i axis and is conjugate

to j_{iz} . In part 2, we chose the x axis to lie along $\mathbf{l} \times \mathbf{k}$ and determined β_1 and β_2 . Here, by choosing the x axis to coincide with the x_2' axis $(\mathbf{j}_2 \times \mathbf{l})$, we have $\beta_2 = 0$ and have only to determine β_1 , the angle between $\mathbf{j}_1 \times \mathbf{l}$ and $\mathbf{j}_2 \times \mathbf{l}$, in terms of J and of the 12-dimensional Monte Carlo point given above. For this purpose the vector identities quoted in part 2 are used:

$$\cos \beta_1 = \frac{\cos \theta_{12} - \cos \theta_{l1} \cos \theta_{l2}}{\sin \theta_{l1} \sin \theta_{l2}}$$
$$\sin \beta_1 = \frac{\sin \theta_{kl} \sin \theta_{12} \sin \alpha_k}{\sin \theta_{12} \sin \alpha_k}$$

$$\sin \beta_1 = \frac{\sin \theta_{kl} \sin \theta_{12} \sin \alpha_k}{\sin \theta_{l1} \sin \theta_{l2}}$$
(A.3)
The Euler angle α_l in eq A.2 is conjugate to l . The conjugate and

 α , or β , and therefore, the internal coordinates r_{mn} , θ_1 , and θ_2 (and hence H_{cl}) are independent of the orientation of the molecule-fixed (x, y, z) system, as stated in the text. Appendix B. Potential V_t for the Transitional Degrees of

contained angles appearing in eq A.1-A.3 are defined in Table

X. None of the Euler angles in eq A.1 and A.2 depend on J_z ,

Freedom Nonbonded Interactions V_{NB} . Between all nonbonded H...H and C...H pairs a Lennard-Jones potential V_{LJ} , given by $\epsilon [(r_0/r)^{12}]$

residual point charges on different atoms were neglected. 53 The resultant nonbonded potential is $V_{\rm NB} = \sum_{m=1}^{4} {'} V_{\rm LJ}(r_{mn})$

 $-2(r_0/r)^6$], was used and Coulomb interactions arising from

where m and n label atoms on different CH_3 fragments and the prime indicates that the C···C contribution is excluded. Bonded Interaction V_B. For the C···C bond formation potential a Morse function was used, modified by an orientational factor to include in an approximate way the influence of the now bent

 $V_{\rm B} = V_{\rm M}^{\rm ef}(r_{\rm CC}) \cos^2 \theta_1 \cos^2 \theta_2$ where an effective potential V_{M}^{ef} was introduced:

C···C bond54

an interpolation:

 $V_{\rm M}^{\rm ef} = D_{\rm CC}^{\rm ef} \{1 - \exp[-\beta_{\rm CC}^{\rm ef}(r_{\rm CC} - r_{\rm CC,e}^{\rm ef})]\}^2 - D_{\rm CC}^{\rm ef}$

Here r_{CC} (= $|\mathbf{r}_{CC}|$) is the carbon-carbon separation distance and

 θ_i is the angle between \mathbf{r}_{CC} and the symmetry axis $z_i^{"}$ of $(CH_3)_i$ The effective Morse parameters in eq B.3 were determined by a least-squares fit of a known C-C Morse function $V_{\rm M}$ to the sum of the potentials $V_{NB} + V_{B}$ given by eq B.1-B.3 and evaluated

along the minimum-energy path from reactants to product. The

latter was obtained by constraining the CH₃ groups to be in the same relative orientation as in equilibrium C_2H_6 ($\theta_1 = 0$, $\theta_2 = \pi$

in eq B.2) and by using the interpolated R-dependent CH₃ structure described below. A least-squares fit over the $r_{\rm CC}$ interval of 1.75–6.78 Å yield a $V_{\rm M}^{\rm ef}$ with a root-mean-square deviation from $V_{\rm M}$ of 0.35 kcal mol⁻¹ for $\alpha = 1.0$ Å⁻¹ and 0.40 kcal mol⁻¹ for $\alpha = 0.8 \text{ Å}^{-1}$. The largest deviations occurred in the 1.75–2.1-Å interval, a region for which the potential was not needed. In the region of interest, namely $r_{\rm CC} \ge 2.2$ Å, $V_{\rm M}^{\rm ef}$ was slightly less

negative than $V_{\rm M}$. In order that the structure of each CH₃ group evolve smoothly when R is varied, from that of an isolated methyl radical to that in C_2H_6 , the local equilibrium carbon-hydrogen bond length r_{CH}

and the H-C-H bond angle α_{HCH} were obtained at each R by

$$r_{\text{CH}}(R) = r_{\text{CH,e}}^{\text{r}} + [r_{\text{CH,e}}^{\text{p}} - r_{\text{CH,e}}^{\text{r}}]g(R)$$

$$\alpha_{\text{HCH}}(R) = \alpha_{\text{HCH,e}}^{\text{r}} + [\alpha_{\text{HCH,e}}^{\text{p}} - \alpha_{\text{HCH,e}}^{\text{p}}]g(R)$$

Here, the superscripts p and r denote product (C₂H₆) and reactant

(isolated CH₃) quantities, respectively. The CH₃ structure and

⁽⁵⁹⁾ Bair, A.; Goddard, W. A., private communication. (60) Kakagawa, I.; Shimanouchi, T. J. Mol. Spectrosc. 1971, 39, 255 (cf.

geometrical deformation of the radicals (planar \rightarrow pyramidal) facilitates the recombination by bringing about a decrease in the exchange repulsion energy.

The parameters appearing in eq B.1 and B.4 as well as other relevant parameters are listed in Table XI. In Figure 1b the various bond angles and bond distances that determine V_t are depicted.

the relative separation and orientation of the two CH₃ groups

together determine the interfragment atomic separations and, hence, V_1 in eq III.4. In addition, the CH₃ structure determines

the three principal moments of inertia $I_A(R)$, $I_B(R)$, and $I_C(R)$,

used to assign a (rigid-rotor) rotational energy to each fragment.

In a theoretical study of the potential energy for colliding methyl radicals, Yamabe, Minato, Fujimoto, and Fukui⁹ found that the

Appendix C. Orientational Analysis of V_{i}

A particular relative separation and orientation of the methyl radicals is achieved from a standard configuration as follows: Consider the two radicals to be superimposed with centers of mass at the origin of the (x, y, z) coordinate system used in section II with the molecular symmetry axes aligned along the z axis. Radical 1 is then translated along the positive z axis by a distance R. The final orientation of radical i (i = 1, 2) is specified by the Euler angles $(\gamma_i, \delta_i, \chi_i)$ which directly connect the (x, y, z) system to the double-primed system (x_i'', y_i'', z_i'') in which the molecular symmetry axis is aligned along the z_i'' axis. χ_i is the rotation in

 z_i'' axes, and γ_i is the rotation in the $x_i''y_i''$ plane about the z_i'' axis $(0 \le \chi_i, \gamma_i \le 2\pi, 0 \le \delta_i \le \pi)$. Since both χ_1 and χ_2 specify rotations in the plane and since

the xy plane about the z axis, δ_i is the angle between the z and

only different values of $\chi_1 - \chi_2$ can yield different relative orientations of the radicals, we simply set $\chi_1 = 0$ and retain χ_2 . This elimination rotations of the entire system about the z axis, thereby reducing the dimensionality of the angular space from six to five. The volume of the five-dimensional angular space can be reduced by taking account of symmetry. Since each radical, as modeled, has C_{3n} symmetry for all R values, γ_i can be confined to the range $0 \le \delta_i \le 2\pi/3$ (i = 1, 2). Furthermore, since the radicals are identical, χ_2 can be restricted to the range $0 \le \chi_2$ $\leq \pi$; values of χ_2 between π and 2π yield configurations different only in the exchange of the two fragments. The range of the angles δ_1 and δ_2 is unaffected by symmetry considerations in this case. The values of these two angles provide a convenient and simplified description of the gross relative orientation of the two radicals: the "back-to-back" orientation with $\delta_1 < \pi/2$ and $\delta_2 > \pi/2$ is denoted configuration A, the "back-to-face" orientation with δ_1 > $\pi/2$ and $\delta_2 > \pi/2$ or $\delta_1 < \pi/2$ and $\delta_2 < \pi/2$ is denoted configuration B, and the "face-to-face" orientation with $\delta_1 > \pi/2$ and $\delta_2 < \pi/2$ is denoted configuration C. A grid with $\Delta \delta_1 = \Delta \delta_2 =$ $\Delta \gamma_1 = \Delta \gamma_2 = \pi/18$ and $\Delta \chi_2 = \pi/9$ proved sufficiently fine for

Registry No. Methyl radical, 2229-07-4.

our examination of V_t .

Reprinted from The Journal of Physical Chemistry, 1987, 91, 4864. Copyright © 1987 by the American Chemical Society and reprinted by permission of the copyright owner.

ADDITIONS AND CORRECTIONS

1986, Volume 90

David M. Wardlaw and R. A. Marcus*: Unimolecular Reaction Rate Theory for Transition States of Any Looseness. 3. Application to Methyl Radical Recombination.

Pages 5383-5393. The factor (2J+1) should be deleted from eq I.3. In eq IV.1, IV.3, and IV.4, the quantity g_c should be in the numerator rather than in the denominator. In Table V, the heading for the fourth column should be $N_{EJ}(R_l^{\dagger})\sigma_l/(2J+1)$, with σ_l as defined in the text (p 5386). In Table IX, the headings for the second and third columns should be $[N_E \pm \sigma^{MC}]\sigma_l/10^{18}$ and $[N_E^{\Lambda} \pm \sigma_{\Lambda}^{MC}]\sigma_l/10^{18}$, respectively.